Residual stress pinning of delamination fronts on polymer-metal interfaces

Vellinga, Willem-Pier; Fedorov, Alexander; De Hosson, Jeff T.

Published in:
Thin Solid Films

DOI:
10.1016/j.tsf.2008.07.020

Publication date:
2008

Thin Solid Films 517 (2008) 841–847

Contents lists available at ScienceDirect

Thin Solid Films

journal homepage: www.elsevier.com/locate/tsf

Residual stress pinning of delamination fronts on polymer–metal interfaces

Willem-Pier Vellinga *, Alexander Fedorov, Jeff T. De Hosson

Department of Applied Physics, Materials Innovation Institute M2i and Zernike Institute for Advanced Materials, University of Groningen, Nijenborgh 4, 9747 AG Groningen, The Netherlands

ARTICLE INFO

Article history:
Received 2 August 2007
Received in revised form 3 June 2008
Accepted 14 July 2008
Available online 25 July 2008

Keywords:
Adhesion
Residual stress
Delamination
Stick-slip

ABSTRACT

The geometry of delamination fronts between a glassy polymer film and a metal substrate in an asymmetric double cantilever beam geometry is studied. Curved crack fronts are observed when tensile residual stresses are present in the polymer layer. Inward bending of the polymer due to the tensile residual stress locally leads to compressive residual stresses normal to the polymer–metal interface and counteracts the imposed crack opening. This modulates the local toughness at the crack front leading to crack front curvature. It is shown that for subcritical cracks under these conditions the critical energy release rate increases with "age" of the crack tip. It also appears that this ageing depends on the local stress state, and that locations with a higher initial toughness age faster. "Pinning points" with increased energy release rates are found to be associated with crack propagation through the polymer layer and also with local stick-slip movement. It is concluded that on these interfaces that are otherwise homogeneous, a distribution of stresses leads to differing local ageing characteristics and delamination mechanisms. The observations indicate that some macroscopic stick-slip phenomena observed in delamination may be due to inhomogeneous front ageing and movement.

1. Introduction

Residual stresses in coatings and multilayers are well-studied phenomena. Stress concentrations near edges are known as initiation sites for delamination and therefore it is important to quantify and preferably control them. This paper illustrates the effect of the residual stress, and residual stress distribution on the geometry of a delamination front on a polymer–metal interface in a Asymmetric Double Cantilever Beam (ADCB) experiment [1]. A sketch drawing of the set-up typical for the experiments discussed here is shown in Fig. 1. The ADCB is a conceptually simple experimental way of studying the adhesion energy or critical energy release rate G_c of bimaterial interfaces. An imposed crack opening Δ leads to a crack with length a. The length a is related to G_c through a straightforward formula (look ahead to Eq. (3) in Section 3.1) that basically results from equating the bending energy per unit length of coating and substrate far behind the crack front and the adhesion energy per unit length far ahead of the crack front. Implicitly it treats the situation as 2-D and it does not take into account residual stresses (see Section 3.1). However, in the ADCB geometry the delamination fronts are not infinitely long but restricted by the width of the samples. It has been established in the literature that in such geometries both residual stresses as well as strong mismatch of elastic properties between film and substrate may give rise to important 3-D effects.

In our case this restriction is shown to have consequences for the front shape, the local energy release rate, local crack propagation mechanisms and local "front ageing" characteristics. A brief discussion of the relevant literature follows below in order to aid interpretation of our results.

The effects of thermal residual stresses on delamination have been studied extensively. The residual stresses and the associated elastic energy in a bimaterial are released when the two parts are separated by a propagating interface crack. The energy release rate G_t associated with the thermal mismatch is

$$G_t = \frac{1-\nu^2}{E_f}\sigma_0^2 h, \tag{1}$$

where σ_0 represents the equi-biaxial thermal residual stress given by

$$\sigma_0 = \frac{E_f \Delta\alpha \Delta T}{1-\nu_f}. \tag{2}$$

Near edges the residual stress is relaxed in the direction perpendicular to the edge. For 2-D situations effective values for the energy release rate of edge cracks of differing length a have been calculated taking this effect into account, e.g. in [2]. In rectangular strips of restricted width w_1 stress relaxation also takes place near the sides resulting in decreasing values of the energy release rate for decreasing w_1. Such 3-D effects on the value of the energy release rate for residually stressed films were studied in detail in [3]. From the point of view of crack propagation the residual stresses are important because they modify the loading mode of the crack front. In 2-D the loading mode is usually discussed in terms of the phase angle ψ

* Corresponding author.
E-mail address: w.p.vellinga@rug.nl (W.-P. Vellinga).

0040-6090/$ – see front matter © 2008 Elsevier B.V. All rights reserved.
doi:10.1016/j.tsf.2008.07.020

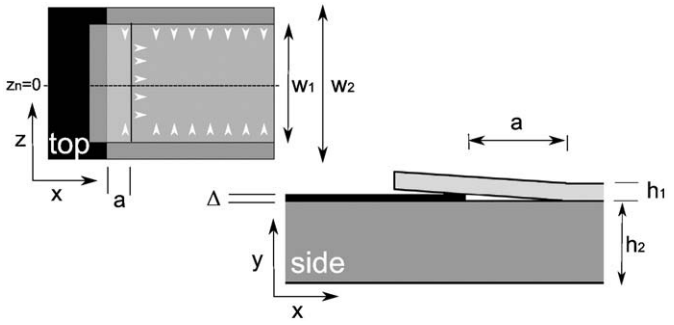

Fig. 1. Sketch of ADCB experiment indicating relevant sizes. White arrows in top-view represent residual tensile stresses in the film. Directly behind the crack front residual stresses along y are not fully released leading to mode III loading of the front.

defined by $\psi=\tan^{-1}(K_{II}/K_I)$ with K_{II} and K_I the mode II and mode I stress intensity factors defined in analogy to those for cracks in isotropic elastically homogeneous media:

$$(\sigma_{22},\sigma_{12}) = (K_1,K_2)\sqrt{2\pi r}, \tag{3}$$

with r the distance ahead of the crack tip. This relation is useful for a qualitative understanding but in fact it is not generally valid as some complications may arise for large elastic mismatch such as in the case treated here. The elastic mismatch between coating and substrate can be characterized by the Dundurs parameters α_D and β_D [4] and Eqs. (3) and (4) strictly only describe cases with $\beta_D=0$. In our case, with a very compliant layer on a stiff substrate, it turns out that $\alpha_D=-0.94$ and $\beta_D=-0.27$. A thorough discussion of the effects of such elastic mismatch for the loading of bimaterial interfaces can be found in [4]. Some results derived there that are specific to this case are used and discussed in more detail in Section 3.1. The mode mixity at the crack tip is determined by these Dundurs parameters, by the ratio between coating and substrate heights $\eta=h_1/h_2$, and by the thermal residual stresses. It has been shown for plane strain situations (such as exist at the centres of wide enough strips) that the presence of residual stress leads to more prominence of the mode II component [5,6] and therefore to a higher absolute value of the phase angle. It is clear from experimental evidence on polymer–polymer and polymer–glass interfaces [e.g. [7,8]] that G_c is strongly mode dependent and that an increase in the mode II component increases G_c.

Near the intersection points of the crack front with free edges mode III components appear as the released coating contracts or expands biaxially, as indicated in Fig. 1. Regardless of the front orientation at the edge this will always lead to mode III loading. It seems reasonable to expect that in-plane and antiplane shear components operating at the crack tip lead to similar (large) effects on G_c and therefore mode III components may be quite relevant. These mode III components and their impact on crack propagation at bimaterial interfaces have been studied in a number of theoretical [e.g. [9–11]] and experimental papers [e.g. [12,13]].

Nakamura [9] treats interface cracks in 3-D bimaterial plates subjected to far field loads. The studies by Begley and Ambrico [10,11] are closer to the situation treated here because they discuss delamination of a residually stressed thin film in tension from corner and edge flaws. In [11] the local energy release rate and stress intensity factors along edge flaw fronts are discussed. The flaws with depth d and width $2w$ consist of circular (with radius Min(d,w)) and straight sections, and both narrow ($d \gg w$) and wide flaws ($d \ll w$) were investigated. Sidestepping complications very close to the corner (distance along front to corner $\ll h$) it is found that for wide shallow flaws the amplitude of all 3 modes varies appreciably near the corners where the crack front intersects the free edge. The local energy release rate therefore also varied considerably along the crack fronts, for wide flaws typically peaking at the edge and passing through a minimum before increasing to constant (approximately plane strain) values near the centre of the flaw. At the same time the loading mode of the flaw front changes as well. Two phase angles $\psi=\tan^{-1}(K_{II}/K_I)$ (introduced before) and $\varphi=\tan^{-1}(K_{III}/K_I)$ are used to describe the loading mode and both are seen to vary near the corner and along curved portions of the crack front. Although many differences exist with our situation the common element in the fronts examined here and in [10] is the intersection of the crack front with a free edge of a film in residual tensile stress. Therefore the main point we derive from these results is that in general near the intersection of a crack front with a free edge the mode mixity and energy release rate differ due to changes in all 3 components. Such modulations of the energy release rate and phase angles are also expected in the case studied here as will be argued in the discussion (Section 3.3).

Information about the importance of the mode mixity on the critical energy release rate needed for delamination can only be derived from experiments. Liechti et al. observed that crack fronts at bimaterial interfaces are usually curved [12] and they suggest that the shape of crack fronts depends on the mode mixity.

In a study of delamination from the base of cuts in polymide films under residual tensile stress on glass substrates Jensen et al. [13] argue that the shape of delaminated areas is expected to be quite sensitive to the mode III contribution to the critical energy release rate. A model parametrizing the mode III contribution to G_c is shown to fit experimental data, and it is concluded that the crack front is shielded from the mode III and mode II contributions in a similar way.

A different type of experimental evidence comes from microscopic observations of crack propagation mechanisms. Swadener et al. [14] and Vellinga et al. [15] showed that instabilities along delamination fronts may clearly show a mode III propagation behaviour, i.e. with protrusions spreading out sideways or with “kinks” travelling parallel to the fronts.

This paper describes the front geometry and the ageing of the front under constant opening amplitude and qualitatively discusses the findings in terms of modulation of the energy release rate and phase angles near the sample edges.

2. Experiment and modeling

Cracks were initiated along a smooth interface (characterized by small amplitude (rms ~ 50 nm) undulations with a lateral size of around 50–100 μm), between Cr (possibly oxidized) and a thick (50 μm after preparation) glycol-modified poly-ethylene terephthalate (PETG) layer (Vivak, Bayer). The Cr layer was deposited on a glass slide in a TEER unbalanced magnetron PVD apparatus. The substrate dimensions were 9 × 60 × 1.15 mm. The glass substrates were soaked in soap, water, methanol, water, acetone, water in this order for 5 min per step in an ultrasonic bath (water refers to water purified by reverse osmosis). Each step was preceded by a rinsing step using the next solvent. Afterwards the glass was blown carefully with compressed dry butane, and heated above 100 °C to dry. The substrates were then glued with silver paste to a sample holder and transferred to the PVD vacuum, 1×10^{-6} (mbar). A cleaning step with high energy Ar^+ ions was performed after which the Cr layer was deposited.

The PETG film was applied at 150 °C under a pressure exerted by spring-loading. To obtain a flat PETG surface, pressure was transferred through a glass slide that was covered with a spin-coated layer of methyl nonafluoro(iso)butyl ether to prevent adhesion to the PETG. The glass parts were backed by metal strips, and the spring-loaded stack was inserted in a heated Al block for 180 (s). Subsequently the sample was left to cool on an oven-stone. After the spring-loaded stack had cooled to room temperature the sample was released. The “fluorinated” glass slide sticks lightly to the top-side PETG but does usually not delaminate spontaneously. The temperature–time profile was measured with a thermocouple in a dummy sample.

The temperature rise can be well described by an empirical function $T_r(t)=T_0+(T_{heat}-T_0)\,(1-e^{-(t-t_0)/t_r})$, (defined for $t>t_0$, the time at which the sample is put in the heating stage) with $t_r=16.6$ (s).

For the cooling we find $T_c(t)=T_r(t)-(T_r(t)-T_0)\,e^{-(t-t_1)/t_d}$ (defined for $t>t_1$ the time at which the sample is put in the heating stage) with $t_d=33.3$ (s). A heating–cooling curve representative for the samples discussed in this paper is shown in Fig. 2.

We have investigated "internal edges" ($w_1<w_2$) rather than "corner edges" ($w_1=w_2$) [2]. Delamination and spalling were observed near corner edges and not near internal edges. This seems to be in contradiction with the findings by Yu et al. [2] who show that corner edges should be more stable against delamination. We assume that the cutting of the glass leads to appreciable stress concentrations at the edges causing local weak spots in the glass.

In the ADCB experiments razor blade (thickness $\Delta=127$ μm) was inserted at the interface between PETG and Cr. The crack front is observed through the PETG [6] on a polarizing optical microscope equipped with a digital camera (1376*1032 pixels).

To study the "ageing" of the crack fronts we have performed "start–stop" experiments similar to those used to measure time-dependent friction properties (pioneered by Dieterich [16]). See Fig. 3. An experiment is initiated by starting the knife at a velocity v_s (~10 μm/s) and allowing the crack front to accelerate to that driving velocity. This step prepares the crack in a reproducible way and can be used to study G_c and crack shape. After a while the knife is stopped at $t=0$. The time during which the knife is stopped is referred to as the "ageing" time hereafter. During this time the crack moves forward a bit, always slowing down indicating that $G_{v=v_s}>G_{v=0}$. At $t=t_w$ the knife starts again and the crack accelerates. In time-dependent friction experiments depending on t_w acceleration (in that case of a block of material on a sliding plane) may take place in a monotonous fashion, but it may also show "stick-slip" character for longer waiting times.

Calculation of the stress distribution was performed using Finite Element Modelling with the open source finite element code Elmer [17] with an isotropic linear elastic material description.

3. Results and discussion

In the following we describe the delamination front shape and the local ageing characteristics. First we discuss briefly the global effects of thermal residual stresses on the ADCB measurements.

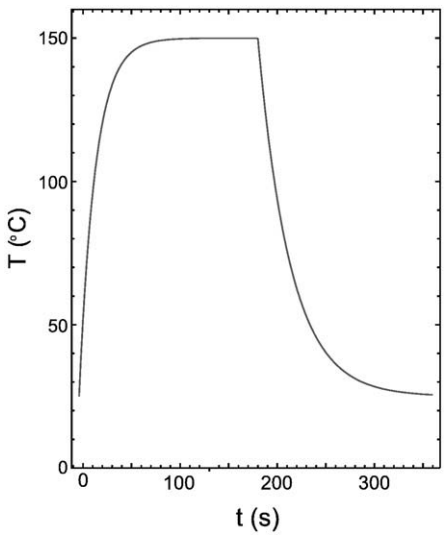

Fig. 2. Temperature-time profile applied during hot-pressing of samples.

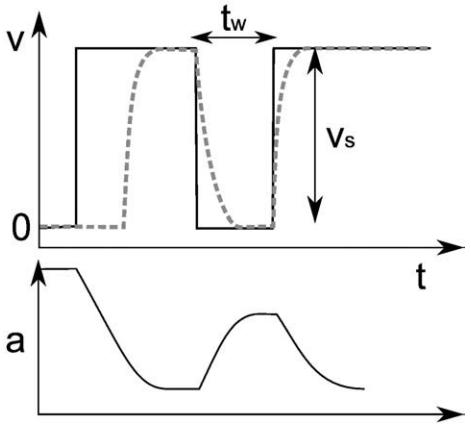

Fig. 3. Sketch of ADCB experiments indicating loading speeds and times of crack fronts.

3.1. ADCB and thermal residual stress

The thermal residual stress impacts the energy release rate G_c of the interface measured in ADCB. Based on the general results in [4] it is possible to derive expressions for the terms on the right hand side in the following formula (see Appendix for a brief explanation)

$$G_c = G_t + G_{tm} + G_m. \tag{4}$$

Here G_c is the energy release rate of the interface. The term G_t constitutes the elastic energy stored in the sample as a consequence of the cooling and the difference in thermal expansion coefficients. G_t is given by (see Appendix for clarification of the symbols):

$$G_t = \frac{c_1}{16}\left(\frac{P_t^2}{Ah_1}+\frac{C_3M_t^2}{Ih_1^3}-\frac{2}{\sqrt{AI}}\frac{C_3P_tM_t}{h_1^2}\sin\gamma\right). \tag{5}$$

This form for G_t does not take into account the stress relaxation near the edges. However, a thin low modulus coating on a high modulus substrate only requires a small correction since the width of the relaxed area near the edges is of the order of the coating height, see Section 3.2. For the samples studied here this leads to an over-estimation of G_t by a factor of approximately $1+h_1/w_1\sim1.05$. This correction is ignored. G_t does not depend on the delamination length a and was calculated to be 4.3 (J/m^2).

The term G_{tm} can be shown to be 0. (In [5,6] this is not stated). This means that the mechanical and thermal contributions are completely separated as far as the determination of the energy release rate G_c is concerned. Of course, the presence of the thermal residual stress does change the mode mixity at the crack tip (see below and [4–6]), and may therefore affect the delamination mechanisms but this is of no consequence for the determination of G_c.

The term G_m constitutes the mechanical energy stored in the bent glass and PETG beams. Recognising that the thermal and mechanical energy contributions in ADCB are separated we use for G_m the formula derived by Kanninen [18], which is an extension of the result by [7] to situations in which $a \gg h_i$ is not valid.

$$G_m = \frac{\left(3\Delta^2E_1E_2h_1^3h_2^3\right)\left(K_2^2E_1h_1^3+K_1^2E_2h_2^3\right)}{8a^4\Lambda^2} \tag{6}$$

with $\Lambda=K_1^3E_2h_2^3+K_2^3E_1h_1^3$ and $K_i=1+0.64\frac{h_i}{a}$.

The crack path is thought to depend on the mode mixity at the crack tip that may be described by the phase angle ψ. For the material combination at hand the elastic mismatch is such that ψ is not constant but depends on the distance ahead of the crack tip $\psi=\psi(r)$. Suo and Hutchinson [4] give a method to calculate ψ (or rather $\psi(h_1)$

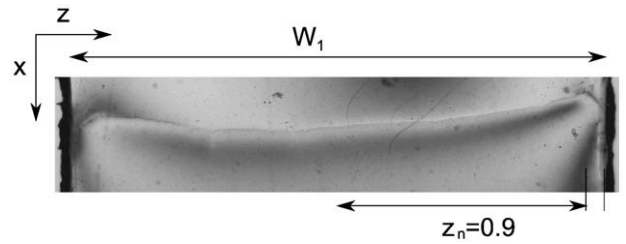

Fig. 4. An experimental (optical polarization) image of a typical static front that was propagated at 10 (μm/s), stopped, and left for 17 (h). The crack propagated from top to bottom.

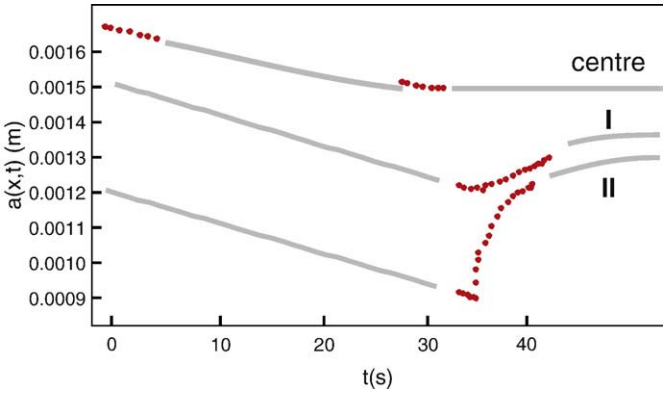

Fig. 6. Front movement at start-up after t_w=17 (h) at three different positions along the crack front: one at a_{max}, one at a_{min} (II), and one on a position in-between (I). Red dots are measurements, grey lines are guides to the eye based on the measured speed of the sample (at low times) and imagined approach of driving speed (at high times). At all positions the front needs appreciable time to reach the driving speed. Interestingly at positions I and II the front overshoots the dynamic equilibrium position and the front speed exceeds that of the blade for some time, it "slips". (For interpretation of the references to colour in this figure legend, the reader is referred to the web version of this article.)

with h_1 the thickness of the film) based on tabulated values of a parameter ω. The case here with α_D=−0.94 and β_D=−0.27 is not covered. However the value of ω is not that sensitive to changes in α_D and β_D, so we extrapolate the values given in [4], where α_D=−0.8 and β_D=−0.27 comes closest and use ω=59°. This leads to a value for the phase angle ψ of (sic) 59°. Without thermal residual stress the value would have been 30°, i.e. appreciably lower. In both cases the positive value of ψ means that the crack is deflected toward the substrate, away from the polymer towards the Cr layer on the glass substrate.

3.2. Observations: delamination front geometry and ageing

At constant knife speed v_s=10 (μm/s) the interface crack propagated along the Cr-PETG interface in a stable way. Fig. 4 shows an experimental image a crack at t_w=17 (h). The almost black areas on both sides of the front are projections of the jagged, cut, edges of the PETG layer. Clearly the crack front is not straight and a single crack extension a cannot be defined. The shape of the front is essentially mirror symmetric with respect to the centreline. Defining a normalised coordinate z_n with respect to the centreline as $z_n = 2z/w_1$ we find for the positions of the minimum and maximum distances to the blade $a_{max}(z_n) \sim a(0)$ and $a_{min}(z_n) \sim a(0.9)$.

Fig. 5 shows another aspect of the pinning. After the blade has stopped, the crack front will propagate at ever decreasing speeds before it stops at some point. This is how the geometry in Fig. 4 has arisen. Now if the blade is started again the front starts moving in the centre first and at the pinning points latest. This is clearly shown in Fig. 6 that shows the front movement at start-up with t_w=17 (h) at three different positions along the crack front: one near the centre, one at a_{min} (labelled II in Fig. 5), and one on a position in-between (labelled I in Fig. 5). At all positions the front is initially static when the blade starts moving. The earliest onset of movement occurs in the centre of the sample. The origin of the time axis in Fig. 6 was chosen to coincide approximately with that moment. At the centre the front slowly picks up speed until it reaches a dynamic equilibrium position a_{v_s} in front of the blade. Meanwhile two forward kinks in the front move sideways to the edges of the sample. At positions I and II the front overshoots a_{v_s} and the front speed exceeds that of the blade for some time, it "slips". At position II this is accompanied by a large jump in position and a speed in excess of $10 \times v_s$. From Fig. 5 it is clear that at positions I and II the crack path runs briefly through the PETG judging from the debris (indicated by the grey line in the Fig. 5) that is left on the interface. Apparently, during ageing the stress release mechanism at the crack front is different from that of the delamination observed at higher speeds. We suggest that at very low speeds shearbands may initiate ahead of the crack tip in the PETG (for experimental evidence pointing to the existence of shearbands see e.g. [19]). When the blade is started again these instabilities may first grow until the material fractures at the moment the "kink" in the crack front moves in from the centre of the sample. Subsequently the crack breaks through to the interface, which is expected based on the phase angle ψ.

It should be emphasized that this is a large effect. The centre part of the front starts moving at a value of a=1.6 (mm) which would correspond to $G_m \sim 20$ (J/m^2) if it were valid for the whole front. a_{min} is equal to 0.9 (mm) corresponding to $G_m \sim 150$ (J/m^2).

The effectiveness of this "pinning" behaviour was also found to depend on the "ageing time" between stopping and starting. For small enough stopping times t_w, the front at position II does not show stick-

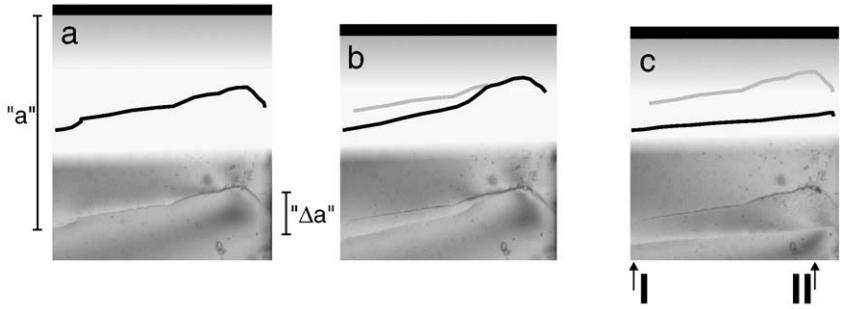

Fig. 5. Experimental images (bottom) from a sequence taken during start-up of a front that had been stopped for 17 (h). The blade (black rectangle of which lower edge indicates blade edge) propagates from top to bottom. Sketches (at the position of already delaminated areas of the front) show front position (black) and position of "debris" left at earlier front position (gray). Note that towards centre of the sample the front moves earlier. "a" indicates length of delaminated area ahead of front, and Δa indicates difference between front position at the side and in the centre.

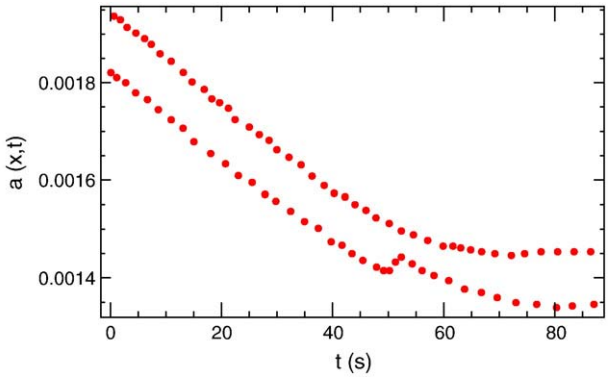

Fig. 7. Front movement at start-up with $t_w = 1$ (h) at positions I and II along the front. No overshooting is visible, $a(x,t) \leq a(x,v_s)$ at all t. Still, at position II a small slip event is observed.

slip, and behaves much like the front at the centre position shown in Fig. 5. This is shown in Fig. 7 which illustrates the start-up of the front after 1 (h) on positions I and II. No overshooting is visible, $a(z) \leq a_{v_s}$ at all t. Still, a difference in behaviour between positions I and II is seen, with a small slip event occurring near position II.

The local ageing characteristics are also impacted by the position along the front. This means that upon start-up the central part of the front moves forward first, after which the initiation of forward movement spreads laterally to the sides. Near the sides locally a "stick-slip" motion of the delamination front may occur. This sequence of events is more pronounced for longer waiting times. The local stick-slip movement is associated with a crack path that travels through the PETG rather than along the interface.

3.3. Discussion

In the introduction it was mentioned that near intersections of cracks and free edges the amplitude of all 3 crack loading modes, the associated phase angles and the energy release rate are modulated [11,13]. We hypothesize that the position dependence of G and the ageing characteristics along the front are caused by such modulations. However, the elastic mismatch in this case is more extreme and we show results of some simple elastic 2-D and 3-D finite element method calculations to qualitatively argue that this is indeed the case.

A 2-D plane strain calculation of the PETG coating on the glass substrate is shown in Fig. 8. It shows the coating (layer 1) under tensile residual stress on top of a substrate (layer 2). Such a situation is commonly encountered where a metal and a polymer are thermally bonded and in that sense it is similar to the situation discussed in [11,13]. In the model system studied here (PETG/Cr-coated-glass) dimensions and temperatures were: $h_1 = 250$ μm, $h_2 = 1150$ μm, $w_1 = 3.5$ mm, $w_2 = 4.5$ mm, $E_1 = 2 * 10^9$ Pa, $E_2 = 70$ GPa, $\alpha_1 = 55 * 10^{-6}$, $\alpha_2 = \alpha_{glass} = 9 * 10^{-6}$, $\Delta T = 423$ K–298 K = 125 K. The Cr layer is very thin (~10 nm) and neglected in the mechanical considerations.

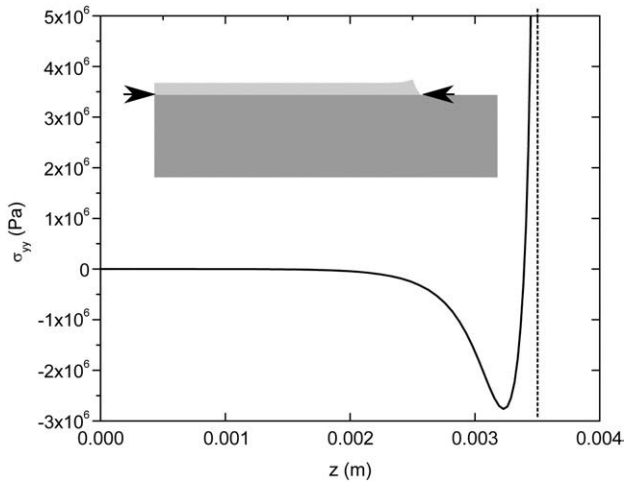

Fig. 8. 2-D plane strain calculation of deformation and normal stress acting at the interface. Compressive stresses occur at the interface close to the free edge.

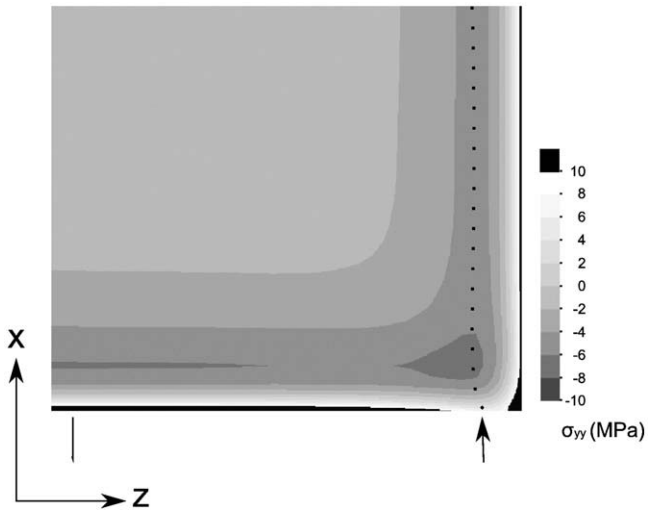

Fig. 9. 3-D calculation of normal stress acting at the interface just ahead of the crack front. Black indicates areas with $\sigma_{yy} > 10^6$ Pa. Arrow indicates a line that roughly follows a "valley" of low values of normal stress. Compressive stress does not occur at the crack front but the opening stress is clearly reduced at the location indicated with the arrow.

Fig. 8 shows the normal stress acting on the interface of such a bimaterial near an edge of the PETG layer. This stress component changes sign some distance away from the edge and in this case it effectively sets up an opening (peeling) moment. It is basically due to the inward bending of the PETG layer due to the action of the residual tensile stress. No analytical solution seems to have been reported for this near-edge stress distribution. The paper by Hsueh et al. [20] offers a simple method to calculate peeling and shear stresses at the very edge of any layer in a multilayer, (assuming $w_1 = w_2$). In the same context they also show Finite Element Modelling results for the stresses on the interface away from the edge. The stress distribution away from the edges is also treated by Yu et al. [2] who use plate theory.

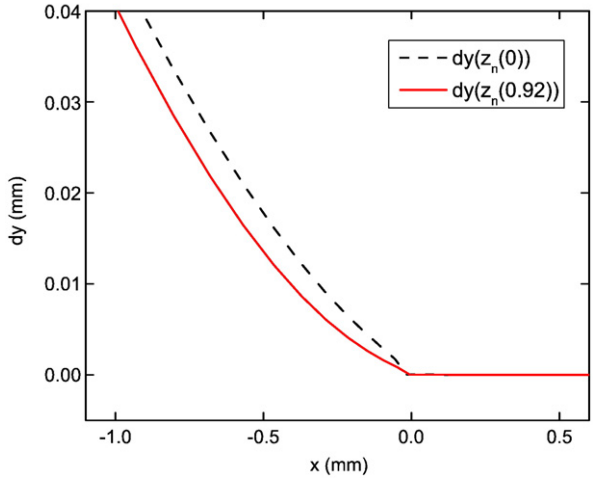

Fig. 10. Crack face displacement dy for two positions along the crack front at the centre and at the position indicated with an arrow in Fig. 9. It is clear that the local crack opening is decreased at the position indicated with the arrow.

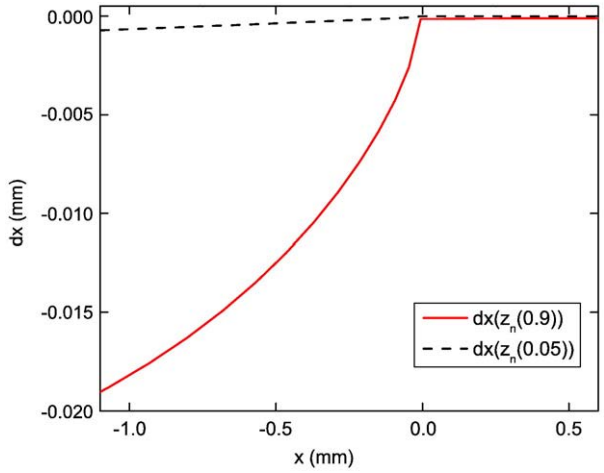

Fig. 11. Crack face displacement d*x* for two positions along the crack front, indicated with a line and an arrow in Fig. 9. Substantial relaxation parallel to the crack front takes place in this geometry indicating presence of the mode III component.

Now imagine a straight crack running beneath a partially released strip of coating as shown in Fig. 1. Near the sides just ahead of the front the free edges will tend to bend inwards as shown in Fig. 8 and are expected to modify (lower) the mode I component of crack loading near the edge. Fig. 9 shows results of 3-D calculations of the normal stress acting on the crack plane ahead of a straight crack on a PETG–glass interface while subjected to an ADCB test with a=2.1 mm (comparable to the value for a in the experimental results). It is evident from the figure that the opening stress is not constant along the front and that the inward bending leads to a decreased amplitude of mode I not just along the side of the sample loading at the crack front as well.

Further away from the front the stress distribution is essentially equal to the 2D situation that was already shown in Fig. 8. Fig. 10 shows the normal displacements dy of the crack face on the PETG side just behind the crack tip, comparing values near the centre with values near z_n(0.9). For the mode I component dy one clearly finds smaller values at z_n(0.9) then at z_n(0), again indicating that the crack is locally closed.

Moreover, in contrast to the 2-D situation the inward deformation just behind the front will give rise to a mode III component. Fig. 11 shows the crack face displacement dx parallel to the crack front at z_n (0.9) and at z_n(0.05) indicating that near the edge there is indeed a clear mode III component to the crack loading.

From these results it is clear that a crack travelling along an interface with a certain restricted width, such as in ADCB experiments, the stress fields associated with the edges of the sample may not only contribute to the mode III component but also to the mode I component of the crack front loading. Specifically in case of the ADCB experiment the inward bending counteracts the applied opening moment supplied by the knife. As a consequence the contribution of mode I to the energy release rate is expected to drop and the phase angles ψ and φ are expected to increase locally. Based on results in the literature a local increase in G_c may therefore be expected at the location where the maximum occurs. The location where the mode I contribution is expected to be at a minimum is consistent with the location of the "pinning" point observed in the experiment.

Slow and subcritical crack propagation may be viewed as a stress-aided thermally activated phenomenon in which the presence of an opening stress decreases the activation barrier for cracking or delamination [21]. The equilibrium front geometry after t_w=17 (h) in Fig. 5 indicates that during relaxation of the front from $a_{v_s}(z)$ to $a_{v_s=0}(z)$ parts of the front that show a larger local value for G_c on average move forward slower which is reasonable.

Inhomogeneous front movement in itself is a well-known phenomenon. On the one hand (e.g. [15,22,23]) it has been observed that at a microscopic scale crack or delamination fronts propagate inhomogeneously in space and time. "Microscopic" here means a length scale below the ones characteristic of the sample. Although present locally the effect of such inhomogeneities (e.g. on a macroscopic measurement of G_c) would average out on the scale of the sample.

On the other hand in peeling experiments macroscopic stick-slip phenomena have been frequently encountered, and it has been suggested for some cases [24] that they may be due to delamination fronts moving inhomogeneously. This has not been established experimentally before, but the present results show that this can indeed be the case.

4. Conclusion

It is concluded that the residual stress distribution near the interface PETG–(Cr-glass) interface determines the curved crack front geometry. Inward bending of the PETG layer counteracts opening of the crack locally close to the free edge. In-plane relaxation behind the crack front leads to substantial mode III loading of the crack front. The combination of these effects is expected to decrease the opening moment and increase the phase angles of loading. Based on the literature a higher local value of G_c would be expected at these locations close to the free edge. The observation of minima for the crack extension a close to the free edge is consistent with such a higher local value of G_c. At the locations with minimum a the crack tip moves forward slower during relaxation of the front towards static equilibrium. The same areas, upon ageing of the crack tip, may show local stick-slip motion. In such cases the delamination front may be "pinned" and briefly propagate as a cohesive crack through the PETG rather than as an adhesive crack along the interface. The pinning is seen to become more effective for longer times. It is suggested that such inhomogeneous movement of the front at the sample scale may occur in other occurrences of stick-slip in delamination that have been reported in the literature.

Appendix A

According to [7] the loading of a crack tip in ADCB experiments can be described using a single moment M and a single force P. These appear in an expression for the energy release rate G:

$$G = \frac{c_1}{16}\left(\frac{P^2}{Ah_1} + \frac{M^2}{Ih_1^3} + \frac{2}{\sqrt{AI}}\frac{PM}{h_1^2}\sin\gamma\right). \tag{A1}$$

For situations with thermal stresses it can be shown that M=M_m−C_3M_t and P=P_t−C_1P_t−(C_2/h_1) M_t. In these expressions M_m is due to the mechanical loading by the blade and M_t and P_t are entirely due to thermal stresses. Combined with Eq. (A1) this gives for G_m, G_{tm} and G_t:

$$G_m = \frac{c_1}{16}\frac{M_m^2}{Ih_1^3} \tag{A2}$$

$$G_t = \frac{c_1}{16}\left(\frac{P_t^2}{Ah_1} + \frac{C_3M_t^2}{Ih_1^3} - \frac{2}{\sqrt{AI}}\frac{C_3P_tM_t}{h_1^2}\sin\gamma\right) \tag{A3}$$

$$G_{tm} = \frac{c_1}{16}\left(-2\frac{C_3M_mM_t}{Ih_1^3} + \frac{2}{\sqrt{AI}}\frac{C_3P_tM_m}{h_1^2}\sin\gamma\right) = 0. \tag{A4}$$

In the previous the following definitions apply:

$$A = \frac{1}{1+(4\eta+6\eta^2+3\eta^3)\Sigma},\ I = \frac{1}{12(1+\eta^3\Sigma)},\ \sin\gamma = 6\eta^2\sqrt{AI(1+\eta)\Sigma},\ \Sigma = \frac{1+\alpha_D}{1-\alpha_D},$$

$$\eta = \frac{h_1}{h_2},\ C_1 = \frac{\Sigma}{A_0},\ C_2 = \frac{\Sigma}{I_0}\left(\frac{1}{\eta} - \frac{\delta}{h_1} + \frac{1}{2}\right),\ C_3 = \frac{\Sigma}{12I_0},\ A_0 = \frac{1}{\eta} + \Sigma,$$

$$I_0 = \frac{1}{3}\left(\Sigma\left(3\left(\frac{\delta}{h_1} - \frac{1}{\eta}\right)^2 - 3\left(\frac{\delta}{h_1} - \frac{1}{\eta}\right) + 1\right) + 3\frac{\delta}{\eta h_1}\left(\frac{\delta}{h_1} - \frac{1}{\eta}\right) + \frac{1}{\eta^3}\right),\ \text{and}\ c_1 = \frac{\kappa_1+1}{\mu_1}$$

with κ_1 the bulk modulus and μ_1 the shear modulus of the coating. M_t and P_t are given by $M_t = \sigma h_1\left(h_2 - \delta + \frac{h_1}{2}\right)$, $P_t = \sigma h_1$, where $\delta = \frac{1+2\Sigma\eta+\Sigma\eta^2}{2\eta(1+\Sigma\eta)}$ and $\sigma = \frac{8\,\Delta\alpha\,\Delta T}{c_1}$ is the difference in thermal expansion coefficient and ΔT the difference between application temperature and final temperature. Inserting $M_m = \frac{\Delta}{4a^2}\left(\frac{E_1 h_1^3 E_2 h_2^3}{(1-\nu_1^2)E_2 h_2^3 + (1-\nu_2^2)E_1 h_1^3}\right)$ in Eq. (A1) leads to Eq. (3) for a h_i.

References

[1] H. Brown, J. Mater. Sci. 25 (1990) 2791.
[2] H. Yu, M. He, J. Hutchinson, Acta Mater. 49 (2001) 93.
[3] H. Yu, J. Hutchinson, Thin Solid Films 423 (2003) 54.
[4] Z. Suo, J. Hutchinson, Int. J. Fract. 43 (1990) 1.
[5] Y. Sha, C. Hui, E. Kramer, S. Hahn, C. Berglund, Macromolecules 29 (1996) 4278.
[6] J. Jiao, C. Gurumurthy, E. Kramer, Y. Sha, C. Hui, P. Borgesen, J. Electron. Packag. 120 (1998) 349.
[7] B. Bernard, H. Brown, C. Hawker, A. Kellock, T. Russell, Macromolecules 32 (1999) 6254.
[8] J. Swadener, K. Liechti, J. Appl. Mech. 65 (1998) 25.
[9] T. Nakamura, J. Appl. Mech. 58 (1991) 939.
[10] M. Begley, J. Ambrico, Int. J. Fract. 112 (2001) 205.
[11] J. Ambrico, M. Begley, Eng. Fract. Mech. 70 (2003) 1721.
[12] K. Liechti, Y. Chai, Y. Liang, Exp. Mech. 32 (1992) 218.
[13] H. Jensen, J. Hutchinson, K. Kim, Int. J. Solids Struct. 26 (1990) 1099.
[14] J. Swadener, K. Liechti, A. de Lozanne, J. Mech. Phys. Solids 47 (1999) 223.
[15] W. Vellinga, R. Timmerman, R. van Tijum, J. De Hosson, Appl. Phys. Lett. 88 (2006) 061912.
[16] J. Dieterich, Pure Appl. Geophys. 116 (1978) 790.
[17] Elmer finite element software. http://www.csc.fi/elmer. downloaded 2007.
[18] M. Kanninen, Int. J. Fract. 9 (1973) 83.
[19] W. Vellinga, R. Timmerman, R. van Tijum, J. De Hosson, Int. J. Solids Struct. 24 (2006) 7371.
[20] C. Hsueh, C. Luttrell, S. Lee, T. Wu, H. Lin, J. Am. Ceram. Soc. 89 (2006) 1632.
[21] S. Santucci, L. Vanel, S. Ciliberto, Phys. Rev. Lett. 93 (2004) 095505.
[22] J. Schmittbuhl, K. Måløy, Phys. Rev. Lett. 78 (1997) 3888.
[23] K. Måløy, J. Schmittbuhl, A. Hansen, G. Batrouni, Int. J. Fract. 121 (2003) 9.
[24] O. Dos Santos Ferreira, PhD. Thesis, University of Technology Eindhoven, The Netherlands (2007).